Segment linkage during evolution of intracontinental rift systems: insights from analogue modelling

T. TENTLER[1] & S. TEMPERLEY[2]

[1]*Hans Ramberg Tectonic Laboratory, University of Uppsala, SE-752 36 Uppsala, Sweden (e-mail: tatiana.tentler@geo.uu.se)*

[2]*Department of Geology, University of Leicester, UK*

Abstract: On the basis of the effective scale-independence of brittle structures, from microcracks to regional fault systems, we have used analogue centrifuge models to provide insights into the initiation and evolution of continental active rifts, with a single dilational fracture segment representing a prototype rift segment. In the models, which are physically and dynamically scaled, a semi-brittle compound material, with flexural rigidity, was devised to simulate the lithosphere as a single layer. This is justified by the fact that, at the largest scale, the lithosphere behaves as a single viscoelastic, flexurally rigid unit. Silicon polymers of two different viscosities and densities represent the asthenosphere. A parallelepiped of lower viscosity and lower density material is embedded within and near the base of the second polymer that fills up most of the model box. The former is activated as a plume-like diapir that rises, spreads laterally and ultimately generates extensional stress in the semi-brittle layer on top. In terms of model fracture distributions, both narrow and wide failure modes were achieved, analogous to narrow and wide modes of rifting. The processes of fracture initiation, propagation and coalescence are the same for each mode. During the early stages of model runs, fracture initiation is more important than the propagation of existing segments in relieving stress, although the latter dominates during later stages. The key parameters of overlap, offset, obliquity and propagation angle, defined and illustrated, are used to distinguish different ways in which pairs of fractures coalesce. We recognize three distinct types of coalescence (type 1, type 2 and type 3) involving both tip-to-tip and tip-to-sidewall linkages. These are described and both graphically and statistically discriminated. Whether narrow or wide mode, an intracontinental rift system consists of a number of discrete fault-bound rift segments. Similar types of interactions to those in the models have been identified between pairs of rift segments from the Cenozoic Baikal and East African rift systems, and the Mesozoic to early Tertiary Central African rift system. The factors that control the type of coalescence between natural rift segments would appear to be precisely those that govern linkages of fracture segments in the models.

Intracontinental rift systems are the result of horizontal extension and associated vertical thinning of continental lithosphere. In terms of causative processes, rifting may be 'active' or 'mantle-activated' when initiated by an upwelling asthenospheric diapir, or else may be 'passive' or 'lithosphere-activated' when generated directly by far-field stresses associated with plate tectonic motions (Sengor & Burke 1978; Turcotte & Emerman 1983; Keen 1985). Irrespective of the fundamental underlying cause, the near-surface expression of a rift is as a composite, elongate graben, bound and dissected by normal faults and variably infilled by volcanic and sedimentary material. Surface heat flow in and around the rift zone is generally high due to plutonic, volcanic and hydrothermal activity, whilst heat flow across the Moho (known as reduced heat flow) is also relatively high, due to the presence of relatively shallow, anomalously hot asthenosphere beneath thinned mantle lithosphere.

Here we define a *rift system* as a series of discrete, variably interlinked *rift segments*. This definition generally holds true whether extension is asthenosphere- or lithosphere-activated, or whether the mode of rifting is wide or narrow (England 1983; Buck 1991; Buck *et al.* 1999). It is, moreover, applicable irrespective of the degree of asymmetry of the fault and shear-zone hierarchies which constitute a rift zone, yielding bulk pure-shear to

From: NIEUWLAND, D. A. (ed.) *New Insights into Structural Interpretation and Modelling*. Geological Society, London, Special Publications, **212**, 181–196. 0305-8719/03/$15

bulk simple-shear model end members (McKenzie 1978; Wernicke 1985; Lister & Davis 1989; Lister *et al.* 1991). In this study, modelling intracontinental active rifting, we are interested in the ways and means by which individual rift segments evolve and interact and, in particular, how the propagation and coalescence of segments result in the development of a through-going intracontinental rift system which, in turn, can lead to continental break-up via a rift-drift transition.

An individual rift segment has finite length and width at the Earth's surface, and may be considered as a zone of extensional deformation accommodated by a population of normal faults and dilational fractures, with one or more zones of ductile flow, although some extension may be accommodated by magmatic accretion and dyking. The scaling characteristics of fault/fracture populations in such zones represents a field of considerable research and debate over the last two decades, with particular emphasis on frequency–length scaling and displacement–length scaling. Studies of cumulative frequency versus fracture length have revealed both power-law and exponential relationships (Poulimenos 2000). The modelling data of Spyropoulos *et al.* (1999) and the field data of Gupta & Scholz (2000) imply a frequency–size transition from power-law to exponential as bulk, brittle fracture-related strain accumulates. The nature of displacement–length scaling represents a more contentious issue. Workers have found both linear and non-linear scaling, with the latter either power-law or exponential (e.g. Cowie & Scholz 1992). However, the most important consequence of scaling in the context of this study is simply that faulting is a self-similar process that has been demonstrated to operate over at least eight orders of magnitude. Because of the fractal characteristics of faulting, small-scale observations of fracture processes, under controlled laboratory conditions, have the potential to yield significant insights into the evolution of much larger-scale, natural fault systems.

How fracture coalescence models for fault zone evolution can throw light on the much larger-scale evolution of an entire rift system remains an important but, as yet, unanswered question. Energy considerations are such that a large-scale fault cannot form all at once, but evolves from interactions at ever-increasing scales. Thus, a graben-defining fault, say between 10 and 100 km in length, will result from the coalescence of smaller-scale segments, which themselves grow by coalescence of even smaller-scale fractures, and so on down to the micro-scale. A system of graben-defining faults constitutes a rift segment, while several, variably linked rift segments define a rift system. The development of an oceanic basin is impossible without prior development of a through-going rift system, the latter demanding progressive coalescence of once-isolated rift segments. When viewed on a continental scale, a rift segment propagates as a single system. Studies of mid-ocean ridges (MOR) at this scale have demonstrated that interactions of ridge rift segments are subject to the same controls as for single faults and small-scale fractures.

Being extremely large-scale, long-lived features, rift systems are not easy to study directly: lengths and widths of individual segments can exceed 1000 and 100 km, respectively, and they evolve over time scales of the order of 10–100 Ma. For these reasons we have turned to physical (analogue) modeling in order to provide insights into rift system evolution. Here we utilize centrifuge-modelling techniques on scaled analogue materials in a three-layer configuration, representing lithosphere, 'normal' asthenosphere and anomalous (i.e. hot) asthenosphere. The scale difference is such that an entire rift segment in nature is represented by a single or composite extensional (mode I) fracture of the lithospheric analogue. The majority of fractures have no discernible shear component and so are purely extensional, opening in a direction perpendicular to their walls, which is the defining characteristic of opening mode, or Mode I cracks (Atkinson 1987). This rationale is directly comparable to that for modelling-based studies of the propagation and linkage of MOR segments (Oldenburg & Brune 1975; Macdonald & Fox 1983; Pollard & Aydin 1984; Shemenda & Grocholsky 1991; Shemenda & Grocholsky 1994; Dauteuil & Brun 1993; Mart & Dauteuil, 2000).

How isolated, individual fracture segments initiate, propagate and coalesce to form a through-going system is illustrated, described and quantified. We present evidence for three types of segment coalescence, and describe and quantify the geometrical factors controlling each type. The results are then compared to natural rift systems representing various stages in rift evolution, where an entire rift basin represents a single segment. Examples chosen for comparison include the Cenozoic Baikal and East African rift systems, together with the Mesozoic to early Tertiary Central African rift system.

Method

Analogue material and scaling

For each experiment, a ductile/brittle model simulating lithosphere and asthenosphere was prepared. Non-linear materials that mimic natural rock deformation and stress distribution were used to construct the model. A strain-softening, semi-brittle material was used to imitate lithosphere. It was pre-

pared as a homogenized mixture of (by weight): 40% paraffin, 33% Vaseline and 27% plaster of Paris, which was heated, stirred when molten and then cooled. Non-linear silicone polymers, with power-law exponents (n) between 1.3 and 4.0, were used to represent the asthenosphere. It is commonly assumed that the asthenosphere behaves as a linear (Newtonian) viscous fluid, particularly at the low deviatoric stress values associated with mantle convection (Lliboutry 1999). However, recent evidence from laboratory experiments suggests that at slightly higher stresses the relationship becomes moderately non-linear, when the effective viscosity would be strongly dependent on temperature, pressure and water content (Davies 1999). For this reason we chose to use non-Newtonian material for simulation of asthenosphere. Polymers of two different rheologies were used. That with the higher viscosity and density is representative of 'typical' subcontinental asthenosphere, while the softer, less dense version represents hotter and more buoyant asthenosphere.

The properties of modelling materials and the dimensions of each material unit of the models are listed in Table 1, together with comparable data for equivalent prototype (natural) units. The rheological properties of the analogue materials were tested in a uniaxial pressure vessel at a constant strain-rate and temperature. The materials were designed or chosen in order to ensure a dynamic equivalence to the physical properties of the natural system. The properties of the analogue materials must therefore satisfy proportional scaling rules, such that the ratios of their stresses, rheologies and densities correspond as closely as possible to those in nature, derived from mechanical, petrological and geophysical data (Hubbert 1937; Ramberg 1981; Weijermars & Schmeling 1986). According to the principles of dynamics and scaling, the following condition must be satisfied:

$$\sigma_r = \rho_r g_r l_r \quad (1)$$

where σ is stress, ρ is density, g is centrifugal (model) or gravitational (natural) acceleration and l is the length-scale. The subscript r indicates that these values are model/prototype ratios (Dixon & Summers 1985; Davy & Cobbold 1991; Brun 1999). The lower densities of the modelling materials compared to natural densities ensures that $\rho_r < 1$. The density of upper asthenospheric mantle varies between 3.38×10^3 and 3.99×10^3 kg m^{-3} (Dziewonski & Anderson 1981). Density values of 3.7×10^3 kg m^{-3} and 3.1×10^3 kg m^{-3} for normal and hot asthenosphere, respectively, yield g_r values of 0.34 and 0.37 (Table 1). While the density of the lithospheric mantle is about 3.3×10^3 kg m^{-3}, that of the crust is lower, between 2.6×10^3 and 3.0×10^3 kg m^{-3}. Rotation of the model increases acceleration, resulting and ensuring that $g_r \gg 1$. The model was rotated in a centrifuge at a speed of 600 rotations per minute, so the acceleration was scaled as $200g$ for model equivalent to $1g$ for prototype. In terms of length scale, 1 mm in the models corresponds to 30 km in nature, and so l_r is extremely small, at 3.3×10^{-8}.

Provided that the model and prototype viscosities are also proportionally scaled, the buoyant forces in the models should correspond to the forces generated in the asthenosphere beneath active rift zones. As a result, the spreading rates in the models should be appropriately scaled to those of natural systems. Assuming non-linear behaviour, viscosity in the mantle appropriate to the time-scale of convection is both temperature- and stress-dependent. The viscosity of the asthenosphere is

Table 1. *Characteristics of analogue materials and model ratios used in the experiments*

Earth unit	Thickness	Density (kg m^{-3})	Viscosity (Pa s) (or other value as stated)
Lithosphere			
Nature	60 km	2.7×10^3	Flexural rigidity: 10^{22}–2×10^{23} Nm
Model	2 mm	1.0×10^3	Strength: 2.5×10^4Pa
Model ratio	0.03	0.37	
Abnormal asthenosphere			
Nature	300 km	3.1×10^3	10^{20}
Model	10 mm	1.1×10^3	3×10^4
Model ratio	0.03	0.35	3×10^{16}
Normal asthenosphere			
Nature	300 km	3.7×10^3	10^{21}
Model	10 mm	1.25×10^3	7.25×10^5
Model ratio	0.03	0.34	7.25×10^{16}

Model ratio is taken as ratio: (parameter in model)/(parameter in nature)

estimated to be between 10^{20} and 10^{21} Pa s (Mitrovica 1996; Lambeck & Johnston 1998), with the lower value more likely to be representative of hotter 'abnormal' asthenosphere. Time-dependent strength variations of the lithosphere imply that it is a viscoelastic unit (a Kelvin–Voight solid) over the time scale appropriate to rifting, with a flexural rigidity of between 10^{22} and 2×10^{23} Nm (Walcott 1970; Cathles 1975).

Modelling procedure and model evolution

Models were constructed so that the density difference in the asthenospheric analogue material would, under the action of centrifugal force, generate a gravitational instability. The technique of centrifuge modelling allows body and surface forces to be scaled with the same ratio, necessary to achieve dynamic similarity of non-Newtonian flows (Mulugeta 1988). First, a rectangular parallelepiped of the lower density polymer was placed centrally at the base of the model box. The dimensions of this unit are illustrated in Figure 1a. Next, the box was filled to within 0.2 cm of the top with the polymer of higher density and viscosity. Finally, an upper planar layer of the semi-brittle material was placed on top. The lateral dimensions of this layer were deliberately made less than those of the confining walls of the box, permitting limited spreading.

The centrifuge technique is particularly suited to deformation of models with small dimensions consisting of high viscosity fluids which can preserve finite deformation and that have fast instability amplification rates. Centrifugal force is employed to increase the apparent gravity field in the analogue materials, and represents the ultimate driving force generating stresses and allowing rapid deformation (Ramberg 1981; Weijermars & Schmeling 1986). Figure 1 illustrates a typical model run. In the centrifuge box, the model was laterally confined from four sides and the base, with the upper surface open. The small gap left around the margins of the upper layer, 1 cm wide, was infilled either with Plasticine or silicon polymer, materials of similar rheology but different strength. They act as soft buffers for the upper layer, limiting the amount of finite extension. Rotation of the model in the centrifuge was interrupted at regular intervals, in order to record the stage of deformation reached, and so provide a semi-continuous history of the development of deformation. After each experiment, the deformed model was removed from the centrifuge and cut vertically, in order to observe and photograph the structure in cross-section.

Stretching of the upper layer was activated by diapiric uprise of the lowest viscosity/lowest density material, analogous to the uprise of a plume of abnormally hot asthenosphere in the mantle. The parallelepiped of this material transforms into a linear plume, which in profile is mushroom shaped (Fig. 1b). Diapiric upwelling leads to divergent lateral flow of the higher viscosity silicon polymer above the plume's head. This in turn generates an extensional stress regime in the upper layer, with $\sigma 1$ vertical and $\sigma 3$ perpendicular to the linear axis of the plume. Amplification of perturbations on the upper surface of the diapir leads to the development of flame-like protrusions that begin to impinge on the lower surface of the upper layer and are responsible for stress concentrations in the latter (Fig. 1c). Thus not only is the regional stress configuration generated from below, but also the local stress anomalies that control positioning of sites of fracture initiation in the semi-brittle layer. Thus the process is analogous to intracontinental active rifting. The ductile, divergent flow above the plume permits further diapiric upwelling that ultimately enhances lateral stretching of the upper layer. As the plume head approaches the base of the upper layer it spreads laterally, while the neck and base of the plume feed progressively into the head, eventually leaving only a short, tapering tail (Fig. 1d). Further stress concentration in the analogue lithosphere results in continued fracturing. The fractures have a significant dilational component, with space between the walls progressively infilled by polymer flowing up towards the model surface (Fig. 1d). The fluid pressure exerted by the polymer on the walls promotes fracture propagation by enhancing dilation and increasing the stress concentration at fracture tips.

The limit of lateral spreading of the upper layer is constrained by two factors: the difference in lateral dimensions between the upper layer and the confining box, and the nature of the material that fills the resultant gap. In the model runs, both Plasticine and rheologically softer polymer were used as fills. Where Plasticine was used, spreading was relatively limited, leading to focused, narrow-mode failure, whereas the less resistant polymer allowed greater finite extension, resulting in diffuse, wide-mode failure. The two failure modes can also be distinguished by a difference in diapir geometry when viewed in cross-section (Fig. 2).

Brittle failure of the upper layer accommodates differential stress build-up induced in the upper part of the model. The fractures that develop are oriented more or less perpendicular to the minimum principal stress and have a dominant tensile component. Fracture arrays are either distributed diffusely across the model surface or are focused within a narrow, linear central zone. Propagation and coalescence result eventually in the development of an interlinked fracture system transecting

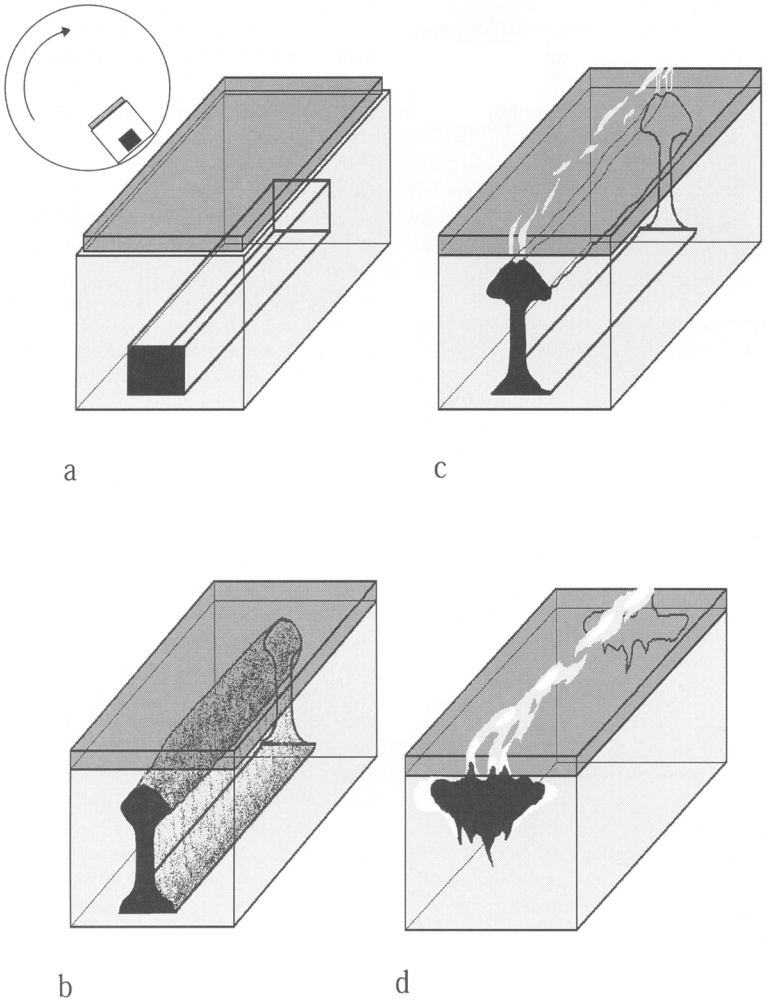

Fig. 1. Block diagrams illustrating the form of the model and successive stages of a typical model run. (**a**) Model configuration. A parallelepiped of lower density, lower viscosity silicone polymer is embedded in a matrix of slightly denser, stiffer polymer. A 2 cm thick sheet of compound, semi-brittle material with flexural rigidity is placed on the top, simulating lithosphere. (**b**) Early stage of model run. The lower density, lower viscosity material is transformed into an upwelling, linear, plume-like diapir by centrifugal acceleration. (**c**) Mid-stage. Divergent, lateral flow of denser, stiffer polymer above upwelling diapir generates extensional stress in upper layer. Stretching of latter leads to development of mode I (tensile) fractures. (**d**) Tail of diapir feeds into head as it spreads beneath upper layer. Stress concentrations lead to further fracturing and increasing dilation of existing fractures, especially above protrusions on upper surface of diapir. Upwelling polymer widens and partially fills the open fractures.

the entire upper surface, either irregular and tortuous (wide mode) or regular and close to rectilinear (narrow mode).

Each experiment was assessed by analysis of both the top, free surface and by cutting cross-sections through the model.

Results

Fracture initiation and propagation

The distributions of fractures across model surfaces are either focused (narrow-mode) or diffuse (wide-

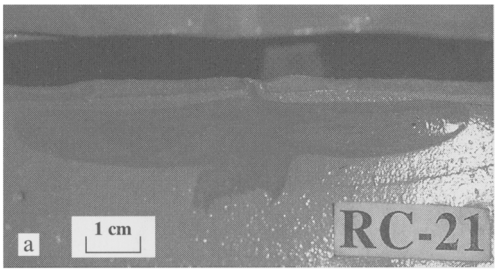

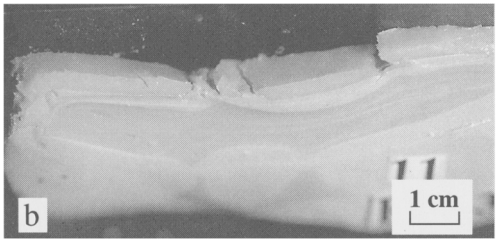

Fig. 2. Cross-sections of models after completion of model runs. (**a**) Example of narrow-mode failure, with only a single, central protrusion of the diapir associated with a focused stress concentration in upper layer. (**b**) Wide-mode failure, with zones of brittle failure in upper layer developed above upward protrusions of diapiric material. Note that the model has collapsed somewhat after removal from the centrifuge.

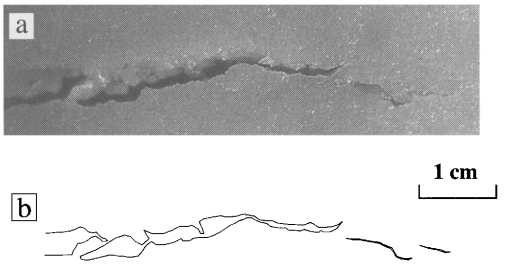

Fig. 3. Plan view of a propagating fracture set on the surface of the upper layer. Newly initiated minor cracks ahead of main tip do not show any opening between their surfaces (far right). As the main fracture propagates, it widens progressively.

mode), depending on the model set-up. In both cases, however, the dynamic and mechanical controls on fracture evolution (i.e. initiation, propagation and linkage) appear to be identical. The upper layer is as homogeneous as we could make it and is effectively isotropic. A single, isolated fracture in such a medium will tend to propagate in-plane, with both strike-parallel (lateral) and subordinate dip-parallel (vertical) components. The fracture is surrounded by a local, elliptical stress perturbation, with two zones of high stress intensity focused on the tips. The stress level is maintained more or less at a critical value as the fracture propagates through the medium. Fracture tips propagate mostly laterally, in a direction perpendicular to local $\sigma 3$, which for dilational structures must be negative (tensile).

Detailed examination of the termination of a fracture segment that has propagated reveals the presence of a damage zone around, and extending well ahead of, the tip (Fig. 3). The zone is characterized by the presence of smaller, secondary cracks (Fig. 3a) that result from the presence of tip-centred stress concentration related to fracture geometry. Some of these are consumed by subsequent migration of the tip, while the more offset cracks that remain tend to close as the fracture propagates through the damage zone (Fig. 3b).

Narrow-mode failure In model runs where spreading of the upper layer is most restricted (by Plasticine fill), the zone of highest stress concentration is relatively narrow (Fig. 4) and is situated immediately above the apex of the upwelling diapir. The upper surface of the plume head has a broad, convex-upward form, with a single, focused further protrusion of diapiric material. The axis of the failure zone in the upper layer is aligned directly above the protrusion. The result is a laterally restricted zone of dilational fractures on the surface of the model (Fig. 4b, stage i). The segments are distributed in a relay pattern, comprising a shingled arrangement of subparallel fractures with no consistent sense of overstep, where all are subparallel to the zone in which they occur.

The limited total width of the array means that lateral offsets between adjacent structures are invariably small (Fig. 4b, stage i), thus the chances of one propagating fracture encountering the stress perturbation of a neighbouring fracture are extremely high. Under such circumstances propagation almost inevitably leads to coalescence, so that very few fractures remain isolated. Adjacent fractures only occasionally propagate tip-to-tip; most pairs overlap each other before mutual tip-to-sidewall coalescence (Fig. 4b, stage ii). The segments that result from coalescence progressively increase in their lengths and widths, while decreasing in number (Fig. 4b, stage iii). The largest segments, of stage iii, coalesce to form a throughgoing system in exactly the same ways that smaller scale linkages were achieved between stages i and ii.

Wide-mode failure With silicon polymer as a peripheral buffer, a greater amount of spreading of the upper layer is permitted. Diapiric impingement and

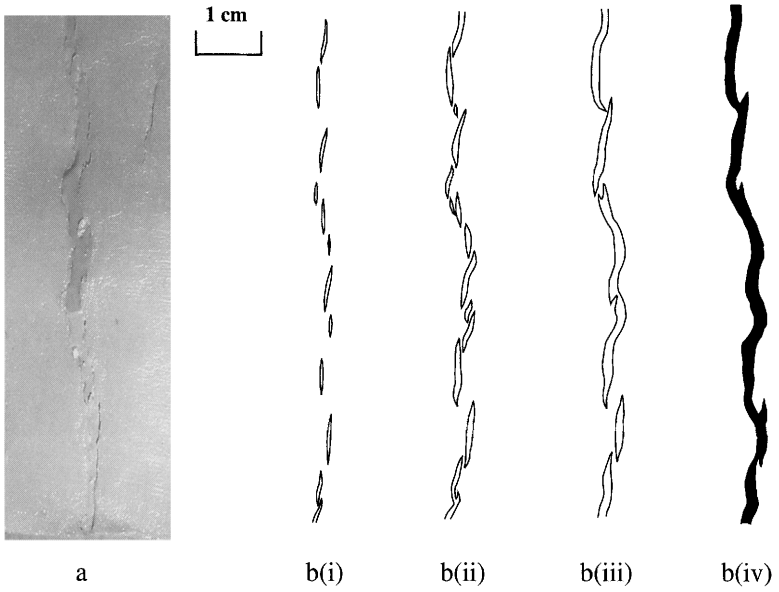

Fig. 4. Narrow-mode failure, in plan view. (**a**) Photograph of upper layer with almost through-going, narrow-mode fracture array. (**b**) Evolution of narrow-mode failure in four stages (i-iv). Sketches depict the initiation, propagation and coalescence of fractures leading to development of through-going, narrow-mode system.

the divergent lateral flow below are initially focused, as for narrow-mode models, generating a central zone of first fractures above the apex of the plume. But as the diapiric spreading phase proceeds, local stress concentrations are induced progressively further away from the central zone (Fig. 5). Because a greater amount of finite extension is permitted in the model set-up, the finite fracture densities are much higher than those from narrow-mode failure. Brittle failure continues apace after initiation of the first fractures, and so the density increases and the distribution widens rapidly (Fig. 5a). Figure 5b illustrates a typical wide-mode run in four stages. At least 80% of the maximum number of fractures have initiated by the end of stage i. They are distributed rather diffusely across the surface of the upper layer, although there is a tendency for fractures to be larger and more densely developed in the axial zone. After stage ii, the density gradually decreases as coalescence proceeds.

As the plume head spreads laterally beneath the upper layer, further instabilities develop spontaneously on its upper surface. A few of these evolve into upward-tapering, flame-like protrusions (Figs 1d and 5a). Since the fracture density is already high by this stage, stress build-up is relieved much more by propagation and dilation of existing structures than by further fracturing (Fig. 5b, stage ii). The dilation of fractures in turn affects the shape of the diapiric body, creating space for further local rises of buoyant material from the protrusions towards the upper surface. The largest and widest fractures are located above the diapiric protrusions and are thus most readily filled by polymer.

Although the mean orientation is more or less parallel to $\sigma 2$, fractures have a much larger strike range than any narrow-mode array. This variability, together with their wide and diffuse distribution, provides the potential for a wider variety of coalescence geometries (Fig. 5b, stage iii). From here onwards, continued growth of the largest and widest fractures relieves most of the stress build-up, so that many of the smaller examples cease to propagate. The dilations of a number of small cracks decrease between stages ii and iv, while a few examples actually close completely. This implies local compression parallel to the stretching direction, in the material between larger dilating fractures, where $\sigma 3$ is positive.

The through-going linked fracture system which results from complete coalescence is highly irregular in geometry, marked by a very wide strike variability from one end to the other, with linked fractures in a zigzag arrangement (Fig. 4b, stage iv). The system also bifurcates into two 'rift arms' over the middle third of its length. A pronounced change in strike of the system is located wherever two markedly oblique segments have coalesced.

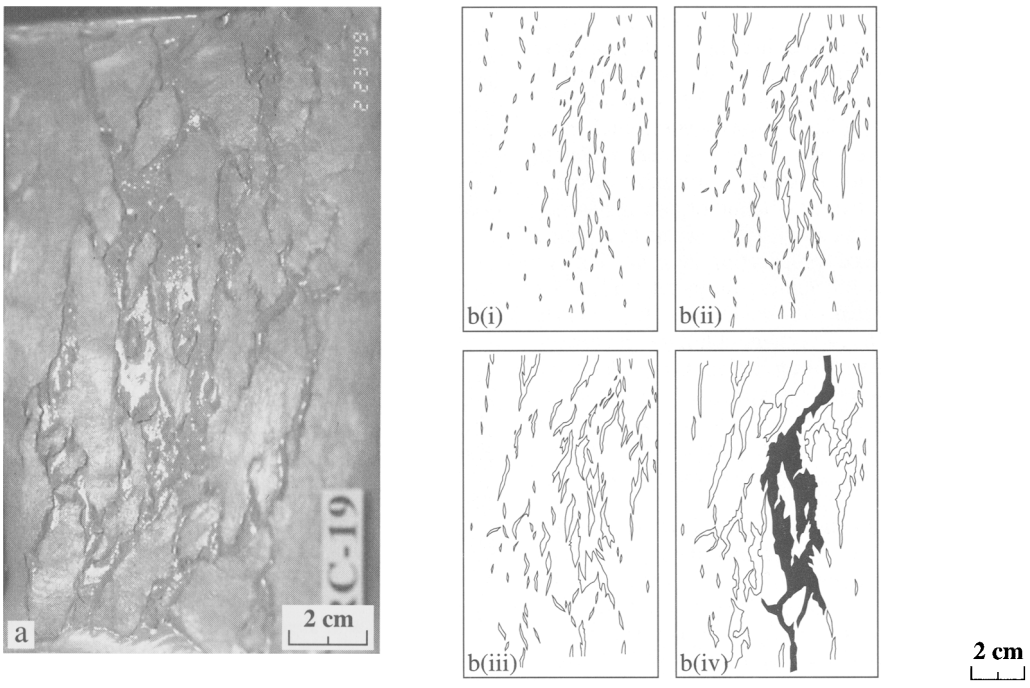

Fig. 5. Wide-mode failure, in plan view. Description corresponds to Figure 4.

Fracture coalescence

If a propagating tip encroaches into the stress perturbation of a neighbouring fracture, it tends to be deflected towards the tip zone or, more usually, the sidewall of the latter. The ensuing coalescence relieves entirely the stress concentration associated with the tip or tips involved in linkage. For a semi-quantitative analysis of the fracture interactions, four particular parameters characterizing the geometries and interrelationships were measured and compared (Fig. 6). The parameters include: *offset*, the minimum separation between fractures; *overlap* of tips, measured parallel to one or both fractures; *obliquity*, the angle between the strikes of two overlapping fractures; and *propagation angle*, the angle between a propagating tip and the fracture it is directed towards.

A linked, through-going failure system represents the amalgamation of a number of discrete fracture sets, each of finite length. The geometry of the system will depend upon the variability of coalescence that, in turn, depends upon the range of individual fracture geometries and the distribution of fractures and fracture arrays. From an examination of fracture evolution on the upper surfaces of models, three types of coalescence have been distinguished between pairs of fractures (Fig. 6).

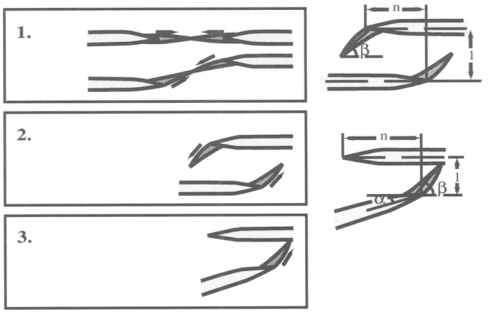

Fig. 6. Coalescence types between pairs of fractures. Two parent fractures (light shading) coalesce by propagation of one or both of their tips (dark shading). (**1**) Type 1 (tip-to-tip) coalescence. (**2**) Type 2 (mutual tip-to-sidewall) coalescence. (**3**) Type 3 (single tip-to-sidewall) coalescence. Parameters used to discriminate coalescence types are defined in the inset diagram. These include: n, overlap; l, offset; α, obliquity; β, propagation angle.

For type 1 coalescence, either a tip of one fracture propagates directly to the tip of another, or the tips of two fractures propagate and link (tip-to-tip interaction in each case). This is possible if offset is small to moderate, obliquity and propagation angle are small or zero and overlap is negative (Fig. 6.1). Types 2 and 3 both involve tip-to-side-

wall interaction. In type 2 coalescence the tips of both fractures are active, but they each propagate along paths that curve in towards the sidewall of the adjacent fracture (double tip-to-sidewall) (Fig. 6.2). In this case, offset and propagation angle may be small or large, overlap positive and moderate to large, and obliquity small to moderate. Type 3 coalescence involves interaction of two non-parallel fractures. In this case, only one tip of a single fracture is activated, propagating in to the flank of the adjacent fracture (single tip-to-sidewall) (Fig. 6.3). It is associated with moderate to large values of overlap, positive overstep, obliquity and propagation angle. As a propagating tip is deflected towards a sidewall during type 2 or type 3 coalescence, the tip angle may approach 90°. At this angle the tip is most unfavourably oriented for dilational propagation, which ceases upon contact with the other fracture.

All three coalescence types in all stages of development may be seen in Figures 4 and 5. It is apparent that good examples of type 1 interaction are less common than those of types 2 or 3. One possible reason for this may lie in the fact that tip-to-tip interaction is not easily recognized in mature rift systems where coalescence obscures any preceding offset. Type 1 coalescence would leave behind a single planar crack, so that recognition of the two former segments would be difficult. This also relates to the fact that determination of type 1 coalescence is rather scale-dependent. Pairs of fractures are rarely perfectly coplanar and rarely have tips that propagate towards each other in precisely the same plane. The width of the tips of fractures is limited so that the chances of precise tip-to-tip linkage are small. It seems, therefore, that most examples of type 1 are in fact extremely small-scale examples of type 2. While examples of types 2 and 3 are commonly observed, they are in fact end members of a continuum of coalescence geometries. In Figures 3 and 4 there are examples intermediate in form between the two types.

Photographs taken during experiments illustrate in more detail the nature of each type of coalescence (Figs 7, 8 & 9). If two adjacent fractures are contained more or less on the same plane and are separated along strike (Fig. 7a), they propagate towards each other by straight paths leading to coalescence that appears as type 1 at the scale of observation (Fig. 7b). The early stage of type 2 coalescence (Fig. 8a) involves equal propagation of both segments. Ideally, the process should leave an 'island' of material upon completion, with segment bifurcation marking the zone of coalescence. More often, however (as in Fig. 8b), only a single arm remains active after coalescence, implying incomplete mutual linkage. Figure 9 shows very clearly the increase in tip angle as type 3 coalescence

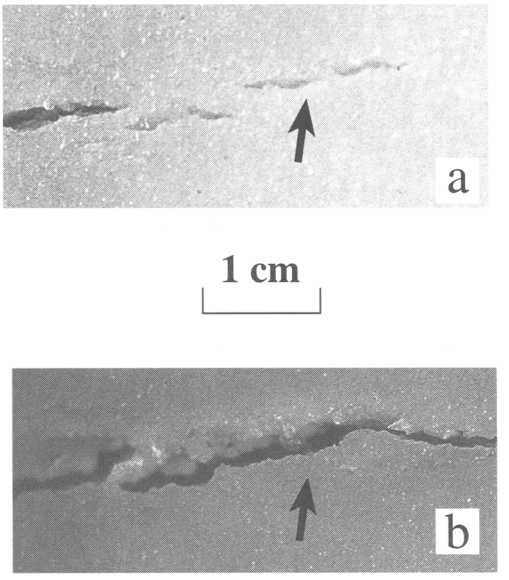

Fig. 7. An example of type 1 coalescence: (**a**) before, and (**b**) after. Location of linkage marked with arrow.

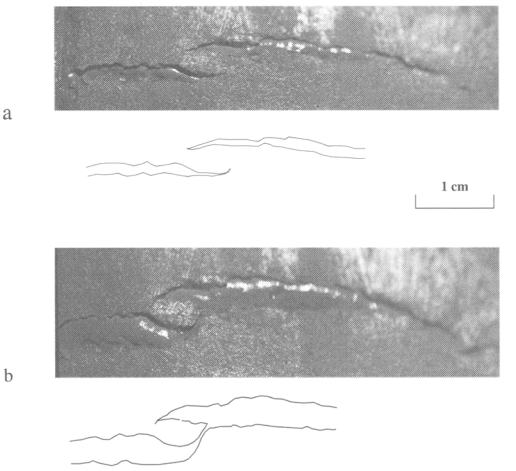

Fig. 8. An example of type 2 coalescence: (**a**) before and (**b**) after. Note that the final stage of coalescence involves only one of the tips propagating to one of the sidewalls, when both tips had been active during the earlier stage.

approaches completion, in this case varying from *c.* 20° as coalescence begins (Fig. 9a), to *c.* 80° on sidewall contact (Fig. 9b).

Precise measurements of segment parameters permit coalescence types to be discriminated graphically (Figs 10 to 13). On a graph of lateral offset versus overlap (Fig. 10), three distinct trends can be observed, each related to a specific type of

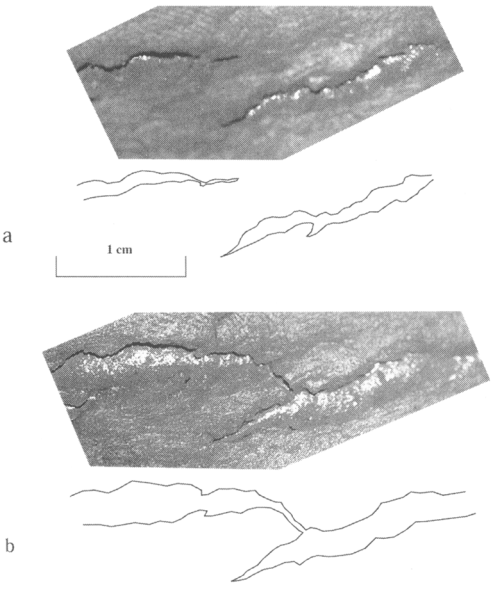

Fig. 9. An example of type 3 coalescence: (**a**) before and (**b**) after.

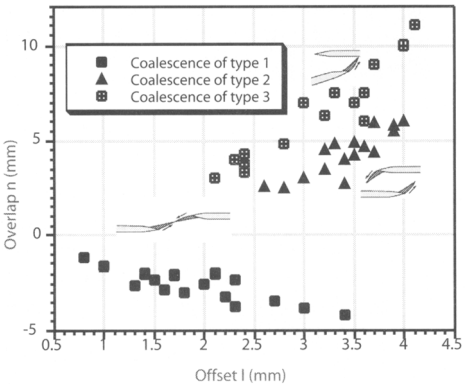

Fig. 10. Graph of offset plotted against overlap, showing differentiation of all three coalescence types.

coalescence. Type 1 is clearly differentiated by negative overlap with variable but mostly small offset values. Types 2 and 3 plot in positive overlap/overstep space, but for a given value of offset, the overlap value is always lower for type 2 than it is for type 3. Thus the degree of overlap appears to be a key factor in controlling whether one or both of the tips will facilitate linkage. A graph of overlap/offset ratio versus frequency (Fig. 11) shows how well the two types of coalescence can be discriminated by means of these parameters. The angular strike difference between two fractures

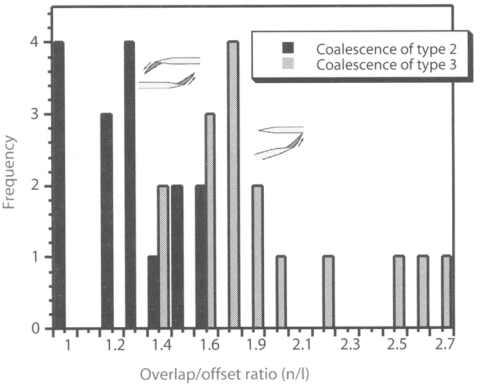

Fig. 11. Differentiation of coalescence types 2 and 3 on a histogram with overlap/offset ratio plotted against frequency.

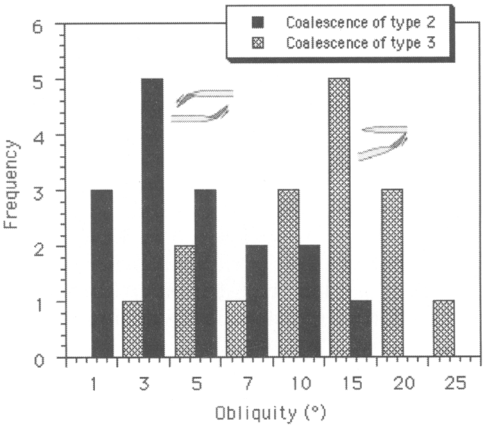

Fig. 12. Coalescence types 2 and 3 plotted on an obliquity versus frequency histogram.

provides a further control for type 2 versus type 3 coalescence. On a plot of this parameter versus frequency (Fig. 12), a prominent bimodal distribution is apparent. This is, in fact, a combination of type 2 and type 3 distributions both displaying skewed unimodal distributions with very different mean values. It may, therefore, be inferred that both tips will propagate where two fractures are subparallel, but only a single tip is likely to be active where the propagation angle exceeds about 10°. A graph of tip angle versus overlap/overstep ratio provides a further discrimination between type 2 and type 3 coalescence (Fig. 13). While plots of each type display a positive rectilinear trend, the ordinate and abscissa values both tend strongly to be lower for type 2 compared to type 3. There is, moreover, a suggestion that, while the values have a small degree of overlap, different

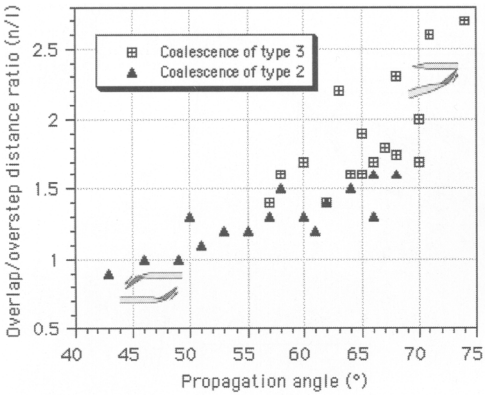

Fig. 13. Differentiation of coalescence types 2 and 3 on a graph of tip-angle plotted against overlap/offset ratio.

slopes define the best-fit lines through their trends. However, the most obvious conclusion is that type 2 coalescence is more likely where tip angles are relatively small, but beyond a tip angle of *c.* 60°, type 3 coalescence is favoured.

Discussion

Limitations of the model

Although we have taken as much care as possible to ensure an accurate scaling between the models and the natural systems, there are certain limitations to be considered. Depth-dependent strength variations are known to be important in controlling the geometry of rift zones. In particular, Benes & Davy (1996), Buck *et al.* (1999) and Brun (1999) have demonstrated that ratio of brittle strength to viscous strength, thickness and thermal state of the lithosphere are likely to be significant factors in narrow-mode versus wide-mode rifting. While none of these factors could be tested in our models, we were nevertheless able to generate both narrow-mode and wide-mode rift systems, by using two materials of different strength as buffers for the lithospheric layer. The buffers controlled the total amount that the lithospheric analogue was allowed to extend, but we see no reason why the value of finite extension should represent an important control over whether a wide or narrow rift develops. However, it may be possible that the *rate* of extension is a function of the rheology of the buffer material, so that the average strain rate in the lithospheric layer of the models is different for narrow-mode and wide-mode model runs. Since the rheology of a material is sensitive to strain-rate, this may represent an important controlling factor, and requires further study.

The modelling was designed to simulate active rather than passive rifting in nature, with the softer of the asthenospheric analogues upwelling as a plume and spreading laterally. Coupling between layers during this spreading phase means that the minimum principal stress, $\sigma 3$, is tensile in the uppermost layer. In nature, on the other hand, $\sigma 3$ is compressive during lithospheric extension, except very close to the surface in some regions. As a result of this limitation, a single tensile fracture in the model cannot be compared to a single normal fault in nature. However, a rift basin segment in nature, with an array of normal faults dipping in towards the axis, possesses a symmetry not unlike that of a single dilational fracture when scaling is taken into consideration. It is of note that significant insights have been achieved through the use of small-scale physical models where a single mode I fracture is analogous to an entire MOR rift segment (Oldenburg & Brune 1975; Pollard & Aydin 1984; Shemenda & Grocholsky 1994; Mart & Dauteuil 2000). Modelling continental lithosphere as a single layer of course represents a considerable oversimplification, but is justified by the scale of the comparison. It is of note that many numerical models of extension, including that for uniform pure shear, first quantified by McKenzie (1978), also assume the lithosphere is a single, uniform mechanical layer, and yet have remained useful for over 20 years in understanding extension on a continent-wide scale.

Comparisons with natural rift systems

Baikal rift system (BRS) The Cenozoic BRS is developed as an arcuate belt of basins on the SE flank of the Siberian craton. The system, which is over 1800 km in length, is superimposed predominantly on a Palaeozoic fold-thrust belt, and flanked to the SE by the Mesozoic Transbaikal orogenic belt (Tapponnier & Molnar 1979; Zonenshain *et al.* 1990) (Fig. 14). Strike-slip faults present at both the NE and SW limits of the rift zone imply the possibility that it is, on the largest scale, a transtensional system. Away from these bounding faults, however, a comparison of the orientations of rift basins with both horizontal principal stress directions and slip vector azimuths (Petit *et al.* 1996) reveal no significant transtensional component. Two main rifting phases have been defined: a slow phase of Oligocene to end early Pliocene age, and a recent, ongoing rapid phase. Total horizontal extension across the BRS is considered to be no more than 10 km (Artyushkov *et al.* 1990).

The Central Baikal rift zone (CBRZ) contains four major rift basins: three deep-water basins of Lake Baikal (South, Central and North Baikal basins) and the Barguzin basin to the east (Fig. 14). Sequences of smaller, variably linked rift basins are

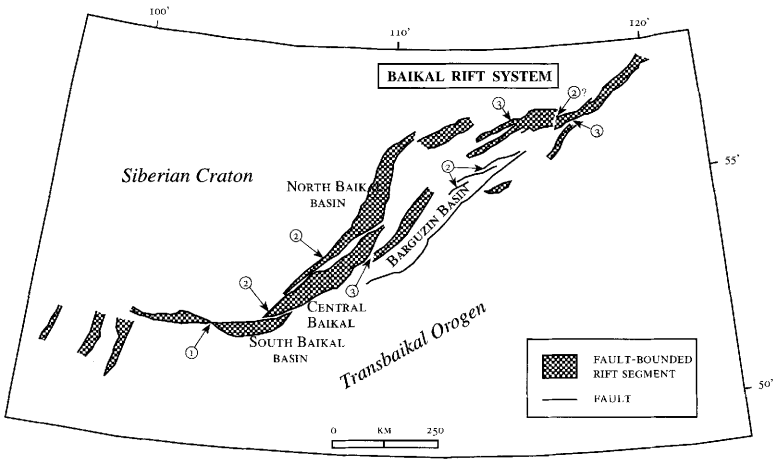

Fig. 14. The Cenozoic Baikal rift system (after Agar & Klitgord 1995) with coalescence types between rift segments marked.

present both to the NE and to the WSW of the four larger segments. In most cases, basins are flanked to the west by a major zone of normal faults, while faults on their eastern flanks tend to be less prominent and to have smaller displacements. Within the central rift zone there is a transition from focused, narrow-mode extension in the SW (the South and Central Baikal basins), to a wider, more diffuse mode to the NE, where the mean elevation is much higher (Fig. 14). Agar & Klitgord (1995) present evidence for broadening of the active Central Baikal rift zone through time, involving propagation and linkage of 10–100 km scale normal faults and the rift segments they define.

At the largest scale, we recognize some 15 discrete segments between 100 and 500 km in length. Pairs of segments display various stages of coalescence and all three types are represented. The more obvious examples of coalescence are highlighted in Figure 14. Within that part of the CBRZ defined by Lake Baikal, the south/central and central/north segment pairs are both good examples of type 2 coalescence that have proceeded almost to completion. The fourth segment, to the east of Lake Baikal, shows incipient type 3 coalescence with the Central Baikal segment. Also shown in Figure 14 are two type 2 interactions between three smaller-scale fault zones.

East African rift system (EARS) Extending from the Afar triple junction in the north to the Zambezi River in the south, the Cenozoic EARS is over 3000 km in length. The system bifurcates in its central portions, around the relatively rigid Tanzania craton that constitutes the East African plateau, with the Tanganyika and Albert rifts in the west, and the Kenya rift in the east (Fig. 15) (Baker & Wohlenberg 1971; Baker *et al.* 1972; Ebinger 1989; Smith 1994). Both the east and west rift arms are superimposed on orogenic belts of Late Proterozoic age, which flank the craton. The earliest phase of rifting, of Pliocene to early Pleistocene age, was the result of east-west directed extension. Although rifting has been more or less continuous to the present day, after early Pleistocene times the extension direction rotated and is now oriented SE-NW (Bosworth & Strecker 1997).

The amount of horizontal crustal extension appears to vary along the system, with values obtained ranging principally between 10 and 40 km. Generally, the rifting has propagated and the rift zone widened southwards through time (Mohr 1982). With evidence of asthenospheric plume activity of Oligocene-Recent age beneath both Afar and the East African Plateau, the east-west to SE-NW extension is generally accepted to be passive. It is also achieved by narrow mode rifting, in the form of two principal, overlapping 'megasegments', each over 1000 km in length, but rarely wider than 100 km. The southern and west-central rift arms are linked to form one megasegment, while the east-central and northern rift arms are linked to form the other (Fig. 15).

At the very largest scale, the configuration of the megasegments is very like that for type 2 coalescence, although at this scale, the rigidity of the Tanzania craton compared to the flanking orogenic belts exerts the principal control on the geometry of the system. The four rift arms themselves each comprise a sequence of discrete, second-order segments, in various stages of coalescence (Fig. 15). The west-central rift arm in particular shows excel-

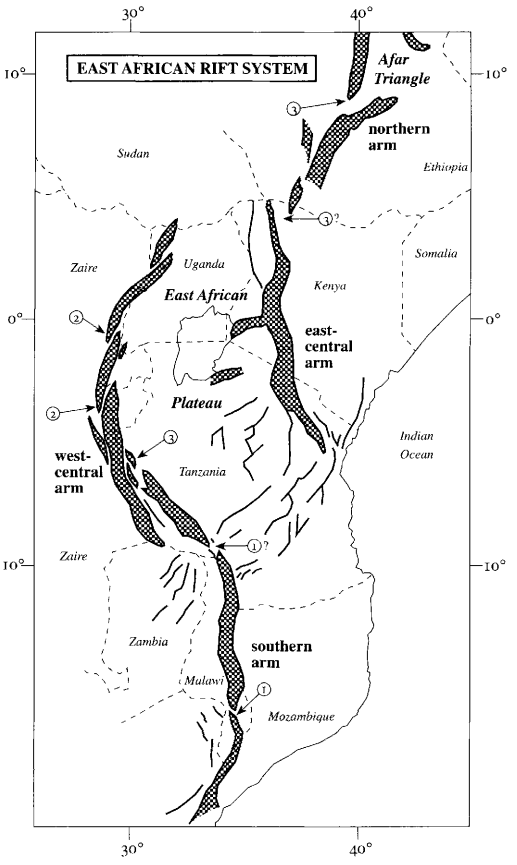

Fig. 15. The Cenozoic East African rift system (after Chapola & Kaphwiyo 1992; Tesha *et al.* 1992) with coalescence types between rift segments marked.

lent examples of type 2 coalescence. Linkages between the southern and west-central arms on the one hand, and the east-central and northern arms on the other, both appear to represent early stages of type 3 coalescence. The three segments that make up the southern arm are linked in two type 1 patterns, while the two main segments of the northern arm show type 3 interaction.

Central African rift system (CARS) Less well known and less obvious than the EARS, but developed on a similar scale, the CARS is the name given to a series of older, inactive SE-NW trending rift segments developed across Kenya and southern Sudan (Fig. 16) (Browne & Fairhead 1983; Browne *et al.* 1985; Fairhead 1988; Bosworth 1992). The system is bounded to the NW by a major NE trending system of dextral strike-slip faults with minor pull-apart basins, the Central African shear zone (Fig. 16). Rift basins are usually flanked on both sides by segmented normal fault systems, the latter accommodating NE-SW directed horizontal extension. The main rifting phase is Mesozoic in age, with evidence of early Tertiary reactivation.

From SE to NW the system changes from narrow mode in Kenya, defined by the Anza rift, to wide mode in southern Sudan, with at least five major, parallel rift zones developed across a region up to 1500 km wide (Fig. 16). The largest of these zones, the Muglad-Abu Gabra rift, is *c.* 100 km wide and up to 1000 km long. The Anza rift is of similar length but is almost 200 km across at its widest. From their geometry, it is evident that the larger examples, including the Anza, Muglad-Abu Gabra, White Nile and Blue Nile rifts, developed by coalescence of smaller-scale segments.

Segment interactions appear to be less clearly defined and coalescence types are not as easily discriminated compared with the BRS and EARS. Transform-like zones of dextral strike-slip within the system, such as the South Sudan shear (Fig. 16), link many pairs of segments. Nevertheless, a few clear examples of direct coalescence can be distinguished of type 2 or type 3 (highlighted in Fig. 16).

Summary of observations

The natural examples of rift segments, from the three systems described above, are taken from both narrow- and wide-mode systems, and include both symmetric graben and asymmetric, detachment-controlled half-graben. The principal factors controlling the type of coalescence between natural rift segments would appear to be precisely those that govern linkages of fracture segments in the models, namely offset and overlap values, together with the difference in trend between two adjacent segments. Of course, the greater lateral restriction of rifts during focused, narrow-mode extension is such that progressive coalescence of segments, to form a through-going system, is likely to be much more readily achieved at low to moderate bulk strains, compared with wide-mode rifting. We would also expect less type 3 interaction between segments, as this would appear to demand offset values and rift-trend differences that are both rather large for narrow-mode rifting.

In two of the three natural examples, the nature of the basement exerts a notable control on the geometry of the system and the distribution of segments. In particular, the siting, orientation and size of segments at the onset of rifting are likely to be strongly controlled by the configuration of basement weaknesses. In this respect, the initial distribution of segments is crucial in determining whether linkage occurs at all and, if so, what type

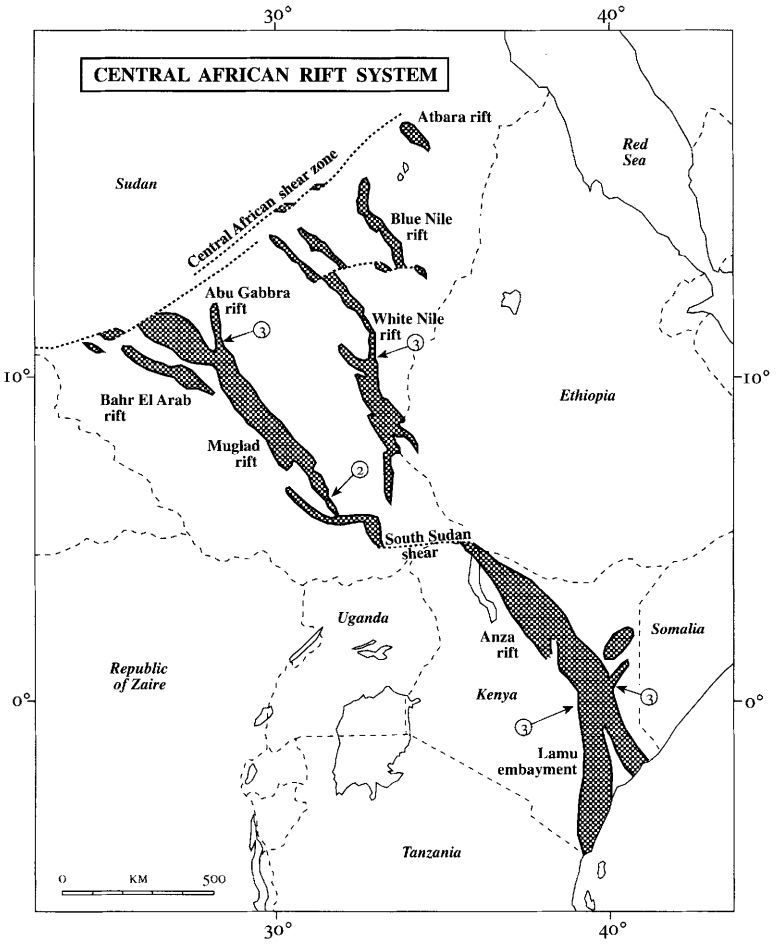

Fig. 16. The Mesozoic to early Tertiary Central African rift system (after Bosworth 1992), with coalescence types between rift segments marked.

of coalescence will take place. If rifting is not sufficiently focused when segments are developing, then the latter will be widely distributed with more chance of isolation and less potential to coalesce unless high bulk strains are achieved.

Conclusions

In the models, there are a limited number of ways in which individual fracture segments amalgamate to form a through-going system. We have outlined three distinct geometries of coalescence between pairs of fractures, involving both tip-to-tip and tip-to-sidewall interactions. These types can be clearly differentiated by comparison of key parameters, including the offset, overlap, obliquity and propagation angle between fracture pairs. In early stages of model runs, fracture initiation is more important than propagation, but the latter dominates during later stages. The final geometry of a linked system and the range of interactions responsible depend ultimately upon the distribution and density of fractures across the model surface. The larger values of offset and obliquity, associated particularly with wide-mode failure, favour type 3 coalescence, although not exclusively so, whereas narrow-mode failure tends to be dominated more by coalescence of types 1 and 2.

Intracontinental rift systems comprise a number of discrete segments, each in the form of a rift basin bounded on one or both sides by normal faults. In order that an ocean basin can eventually develop, flanked by passive continental margins, a linked, through-going system of terrestrial rift segments must evolve. Analysis of the Baikal, East African and Central African active rift systems

reveals precisely the same three types of interactions between pairs of rift segments, controlled by the same parameters as those defined for fracture segments in the models. These natural examples include elements of both narrow-mode and wide-mode rifting, with the former dominated by types 1 and 2 coalescence and the latter by type 3.

The authors would like to thank G. Mulugeta for advice on experimental design and for helpful suggestions during the modelling.

References

AGAR, S. M. & KLITGORD, K. D. 1995. Rift flank segmentation, basin initiation and propagation: a neotectonic example from Lake Baikal. *Journal of the Geological Society, London,* **152**, 849–860.

ARTYUSHKOV, E. V., LETNIKOV, F. A. & RUZHICH, V. V. 1990. The mechanism of formation of the Baikal basin. *Journal of Geodynamics,* **11**, 277–291.

ATKINSON, B. K. 1987. Introduction to Fracture Mechanics. *In*: ATKINSON, B. K. (ed.) *Fracture Mechanics of Rock*. Academic Press, London.

BAKER, B. H. & WOHLENBERG, J. 1971. Structure and evolution of the Kenya rift valley. *Nature,* **229**, 538–542.

BAKER, B. H., MOHR, P. A. & WILLIAMS, L. A. J. 1972. *Geology of the eastern rift system of Africa*. Geological Society of America, Special Papers, **136**.

BENES, V. & DAVY, P. 1996. Modes of continental lithospheric extension: experimental verification of strain localization processes. *Tectonophysics,* **254,** 69–87.

BOSWORTH, W. 1992. Mesozoic and early Tertiary rift tectonics in East Africa. *Tectonophysics,* **209**, 115–137.

BOSWORTH, W. & STRECKER, M. R. 1997. Stress field changes in the Afro-Arabian rift system during the Miocene to Recent period. *Tectonophysics,* **278**, 47–62.

BROWNE, S. E. & FAIRHEAD, J. D. 1983. Gravity study of the Central African rift system: a model of continental disruption 1. The Ngaoundere and Abu Gabra Rifts. *Tectonophysics,* **94**, 187–203.

BROWNE, S. E., FAIRHEAD, J. D. & MOHAMED, I. I. 1985. Gravity study of the White Nile Rift, Sudan and its regional tectonic setting. *Tectonophysics,* **113**, 123–137.

BRUN, J-P. 1999. Narrow rifts versus wide rifts: inferences for the mechanics of rifting from laboratory experiments. *Philosophical Transactions of the Royal Society of London,* **357**, 695–712.

BUCK, W. R. 1991. Modes of continental lithospheric extension. *Journal of Geophysical Research,* **96**, 20161–20178.

BUCK, W. R., LAVIER, L. L. & POLIAKOV, A. N. 1999. How to make a rift wide. *Philosophical Transactions of the Royal Society of London,* **357**, 671–693.

CATHLES, L. M. 1975. *The Viscosity of the Earth's Mantle*. Princeton University Press, Princeton.

CHAPOLA, L. S. & KAPHWIYO, C. E. 1992. The Malawi rift: geology, tectonics and seismisity. *Tectonophysics,* **209**, 159–164.

COWIE, P. A. & SCHOLZ, C. H. 1992. Displacement to length scaling relationships for faults: Data synthesis and discussion. *Journal of Structural Geology,* **14**, 1149–1156.

DAUTEUIL, O. & BRUN, J-P. 1993. Oblique rifting in a slow-spreading ridge. *Nature,* **361**, 145–148.

DAVIES, G. F. 1999. *Dynamic Earth*. Cambridge University Press, Cambridge.

DAVY, P. & COBBOLD, P. R. 1991. Experiments on shortening of a 4-layer model of the continental lithosphere. *Tectonophysics,* **188**, 1–25.

Dixon, J. M. & SUMMERS, L. M. 1985. Resent developments in centrifuge modelling of tectonic processes: equipment, model construction techniques and rheology of modern materials. *Journal of Structural Geology,* **7**, 83–102.

DZIEWONSKI, A. M. & ANDERSON, D. L. 1981. Preliminary reference earth model. *Physics of the Earth and Planetary Interiors,* **25**, 297–356.

EBINGER, C. J. 1989. Geometric and kinematic development of border faults and accommodation zones, Kivu-Risizi rift, Africa. *Tectonics,* **8**, 117–133.

ENGLAND, P. 1983. Constraints on the extension of continental lithosphere. *Journal of Geophysical Research,* **88**, 1145–1152.

FAIRHEAD, J. D. 1988. Late Mesozoic rifting in Africa. *In*: MANSPEIZER, W. (ed.) *Triassic-Jurassic Rifting*. Elsevier, Amsterdam, Developments in Geotectonics, **22**, 821–831.

GUPTA, A. & SCHOLZ, C. 2000. Brittle strain regime transition in the Afar depression: Implications for fault growth and seafloor spreading. *Geology,* **28**, 1087–1090.

HUBBERT, M. K. 1937. Theory of scale models as applied to the study of geologic structures. *Bulletin of the Geological Society of America,* **48**, 1459–1519.

KEEN, C. E. 1985. The dynamics of rifting: deformation of the lithosphere by active and passive driving forces. *Geophysical Journal of the Royal Astronomical Society,* **80**, 95–120.

LAMBECK, K. & JOHNSTON, P. 1998. The viscosity of the mantle: evidence from analyses of glasial rebound phenomena. *In*: JACKSON, I. N. S. (ed.) *The Earth's Mantle: Composition, Structure and Evolution*. Cambridge University Press, Cambridge, 461–502.

LISTER, G. S. & DAVIS, G. A. 1989. The origin of metamorphic core-complexes and detachment faults formed during Tertiary continental extension in the northern Colorado River region. *Journal of Structural Geology,* **11**, 65–94.

LISTER, G. S., ETHERIDGE, M. A. & SYMONDS, P. A. 1991. Detachment models for the formation of passive continental margins. *Tectonics,* **10**, 1038–1064.

LLIBOUTRY, L 1999. *Quantitative Geophysics and Geology*. Springer-Verlag, Berlin.

MACDONALD, K. C. & FOX, P. J. 1983. Overlapping spreading centres: A new kind of accretion geometry on the East Pacific Rise. *Nature,* **302**, 55–58.

MCKENZIE, D. 1978. Some remarks on the development of sedimentary basins. *Earth Planetary Science Letters,* **40**, 25–32.

MART, Y. & DAUTEUIL, O. 2000. Analogue experiments of propagation of oblique rifts. *Tectonophysics,* **316**, 121–132.

MITROVICA, J. X. 1996. Haskell [1935] revised. *Journal of Geophysical Research,* **101**, 555–569.

MOHR, P. 1982. Musings on continental rifts. *In*: PALMASON, G. (ed) *Continental and Oceanic Rifts*. American Geophysical Union, Geological Society of America, Geodynamic Series, **8**, 293–309.

MULUGETA, G. 1988. Squeeze box in a centrifuge. *Tectonophysics,* **148**, 323–335.

OLDENBURG, D. W. & BRUNE, J. N. 1975. An explanation for the orthogonality of ocean ridges and transform faults. *Journal of Geophysical Research,* **80**, 2575–2585.

PETIT, C., DEVERCHERE, J., HOUDRY, F., SANKOV, V. A., MELNIKOVA, V. I. & DELVAUX, D. 1996. Present-day stress field changes along the Baikal rift and tectonic implications. *Tectonics,* **15**, 1171–1191.

POLLARD, D. D. & AYDIN, A. 1984. Propagation and linkage of oceanic ridge segments. *Journal of Geophysical Research,* **89**, 10017–10028.

POULIMENOS, G. 2000. Scaling properties of normal fault populations in the western Corinth Graben, Greece: Implications for fault growth in large strain settings. *Journal of Structural Geology,* **22**, 307–322.

RAMBERG, H. 1981. *Gravity, Deformation and the Earth's Crust* (second edition). Academic Press, London.

SENGOR, A. M. C. & BURKE, K. C. 1978. Relative timing of rifting and volcanism on Earth and its tectonic implications. *Geophysical Research Letters,* **5**, 419–421.

SHEMENDA, A. I. & GROKHOLSKY, A. L. 1991. A formation and evolution of overlapping spreading centers (constrained on the basis of physical modeling). *Tectonophysics,* **199**, 398–404.

SHEMENDA, A. I. & GROCHOLSKY A. L. 1994. Physical modeling of slow seafloor spreading. *Journal of Geophysical Research,* **99**, 9137–9153.

SMITH, M. 1994. Stratigraphic and structural constraints on mechanisms of active rifting in the Gregory Rift, Kenya. *Tectonophysics,* **236**, 3–22.

SPYROPOULOS, C., GRIFFITH, W. J., SCHOLZ, C. H. & SHAW, B. E. 1999. Experimental evidence for different strain regimes of crack populations in a clay model. *Geophysical Research Letters,* **26**, 1081–1084.

TAPPONNIER, P. & MOLNAR, P. 1979. Active faulting and Cenozoic tectonics of the Tien Shan, Mongolia and Baikal regions. *Journal of Geophysical Research,* **84**, 3425–3459.

TESHA, A. L., EBINGER, C. J. & NYAMWERU, C. 1992. Rift-related volcanic hazards in Tanzania and their mitigation. *Tectonophysics,* **209**, 277–279.

TURCOTTE, D. L. & EMERMEN, S. H. 1983. Mechanisms of active and passive rifting. *Tectonophysics,* **94**, 39–50.

WALCOTT, R. J. 1970. Flexural rigidity, thickness, and viscosity of the lithosphere. *Journal of Geophysical Research,* **75**, 3941–3954.

Weijermars, R. & SCHMELING, H. 1986. Scaling of Newtonian and non-Newtonian fluid dinamics without inertia for quantitative modelling of rock flow due to gravity (including the concept of rheological similarity). *Physics of the Earth and Planetary Interiors,* **43**, 316–330.

WERNICKE, B. 1985. Uniform-sense normal simple shear of continental lithosphere. *Canadian Journal of Earth Science,* **22**, 108–125.

ZONENSHAIN, L. P., KUZMIN, M. I. & NATAPOV, L. M. 1990. *Geology of the USSR: A Plate-tectonic Synthesis*. American Geophysical Union, Geodynamics Series, **21**.